Princeton Plasma Physics Laboratory

PPPL- 4801

PPPL- 4801

The Effects of the Scattering by Edge Plasma Density Fluctuations on Lower Hybrid Wave Propagation

N. Bertelli, G. Wallace, P.T. Bonoli, R.W. Harvey, A.P. Smirnov, S.G. Baek, R.R. Parker, C.K. Phillips, E.J. Valeo, J.W. Wilson and J.C. Wright

August, 2012

PPPL PRINCETON PLASMA PHYSICS LABORATORY

Prepared for the U.S. Department of Energy under Contract DE-AC02-09CH11466.

Princeton Plasma Physics Laboratory
Report Disclaimers

Full Legal Disclaimer

Trademark Disclaimer

PPPL Report Availability

Princeton Plasma Physics Laboratory:

http://www.pppl.gov/techreports.cfm

Office of Scientific and Technical Information (OSTI):

http://www.osti.gov/bridge

Related Links:

U.S. Department of Energy

Office of Scientific and Technical Information

Fusion Links

The effects of the scattering by edge plasma density fluctuations on lower hybrid wave propagation

N. Bertelli[1], G. Wallace[2], P. T. Bonoli[2], R. W. Harvey[3], A. P. Smirnov[4], S. G. Baek[2], R. R. Parker[2], C. K. Phillips[1], E. J. Valeo[1], J. R. Wilson[1], J. C. Wright[2]

[1]Princeton Plasma Physics Laboratory, Princeton, NJ 08543 USA
[2]MIT Plasma Science and Fusion Center, Cambridge, MA 02139, USA
[3]CompX, Del Mar, CA 92014, USA
[4]Lomonosov Moscow State University, Moscow, Russia

E-mail: nbertell@pppl.gov

Abstract. Scattering effects induced by edge density fluctuations on lower hybrid (LH) wave propagation are investigated. The scattering model used here is based on the work of Bonoli and Ott [Phys. Fluids **25** (1982) 361]. It utilizes an electromagnetic wave kinetic equation solved by a Monte Carlo technique. This scattering model has been implemented in `GENRAY`, a ray tracing code which explicitly simulates wave propagation, as well as collisionless and collisional damping processes, over the entire plasma discharge, including the scrape-off layer (SOL) that extends from the separatrix to the vessel wall. A numerical analysis of the LH wave trajectories and the power deposition profile with and without scattering is presented for Alcator C-Mod discharges. Comparisons between the measured hard x-ray emission on Alcator C-Mod and simulations of the data obtained from the synthetic diagnostic included in the `GENRAY/CQL3D` package are shown, with and without the combination of scattering and collisional damping. Implications of these results on LH current drive are discussed.

1. Introduction

Because lower hybrid current drive (LHCD) is one of the most efficient methods for driving current non-inductively in magnetically confined plasma, it can play an important role for current profile control and instability suppression for the advanced tokamak regime in devices such as Alcator C-Mod and ITER [1]. Though the propagation of LH waves in tokamaks has been intensively studied in the past few decades, there are still some unresolved issues. In addition to the well-known spectral gap problem [2], the most recent one is related to an apparent "density limit" in which the efficiency of LHCD decreases at high plasma density [3]. The underlying cause of this "density limit" could be strong interactions between the LH waves and the scrape off layer (SOL) and, in fact, several publications go in this direction. However, it is still an open question exactly which physical mechanism or the combination of different mechanisms is responsible. Many explanations have been proposed, such as parametric instabilities [4, 5], collisions [3, 6], full wave effects [7, 8] and scattering induced by the plasma density fluctuations [9]. In this work, the role of edge plasma density fluctuations on the scattering and collisional damping of the LH waves is evaluated by implementing a more complete model for the scattering into the ray-tracing code `GENRAY` [10]. Unlike the recent work [9] based on the Andrews and Perkins model [11] and other studies based on a statistical description of the electron density fluctuations [12] and a Fokker-Planck formalism [13], scattering effects included here are based on the model of Bonoli and Ott [14, 15] that introduces an electromagnetic wave kinetic equation solved by a Monte Carlo technique. This model has been also adopted for studying the effects of magnetic fluctuations on LH wave propagation [16]. Scattering of the waves off of density fluctuations can enhance LH wave penetration into the plasma core, due to the $k_{\|}$ upshift through the poloidal field (because of the rotation of $k_{\perp}$ that provides a finite poloidal mode number). Scattering can also inhibit the wave penetration for high edge density due to enhanced collisional losses from rays spending more time in the SOL. Because the earlier studies [14, 15] were done in circular, limited discharges with low ray statistics, it is important to re-evaluate the scattering effects for Alcator C-Mod, utilizing modern computational capabilities to include a larger number of rays for the wave propagation and damping, as well as a detailed numerical fit to the plasma equilibrium that encompasses the region between the magnetic axis and last closed flux surface (LCFS), and the SOL region, outside of the separatrix. In this work we have included the effects of scattering in the ray tracing code `GENRAY`, which also computes collisional damping effects both inside the separatrix, where collisional damping is small relative to Landau damping, and in the SOL, where collisional damping may be more significant. The ray paths and the power deposition from `GENRAY` are then used in the bounce averaged Fokker-Planck solver `CQL3D` [17] to calculate the perturbed electron distribution function and the quasilinear wave absorption inside the LCFS. `CQL3D` includes a fast electron bremsstrahlung x-ray synthetic diagnostic that can be used to compare the simulation with the experimental observations.

The purpose of this paper is to describe the implementation of this particular scattering model in a ray tracing code, to discuss the effects of scattering on LH wave propagation and absorption and to compare the model predictions with the experimental observations of the hard x-ray spectrum generated by the LH wave interaction with plasmas on the Alcator C-Mod tokamak. The paper is structured as follows: the derivation of the wave kinetic equation describing the effects of the scattering by the plasma density fluctuations is reviewed and summarized in Section 2. Validity of the wave kinetic equation together with a description of the main steps for solving this equation by a Monte Carlo technique (as implemented in the ray tracing code `GENRAY`) are also presented. Results from the model are discussed in Section 3, where single ray trajectories are presented in order to illustrate the possible scattering effects on LH propagation. The predicted power density profiles with and without scattering are also shown, for different Alcator C-Mod discharges. A comparison between the predictions from the synthetic diagnostic included in the `GENRAY/CQL3D` package and the experimental hard x-ray data from Alcator C-Mod is presented. Finally, a discussion of these results and the conclusions are given in Section 4.

2. The lower hybrid scattering model

2.1. The wave kinetic equation with density fluctuations

In order to investigate LH wave propagation and the absorption in the presence of density fluctuations, Bonoli and Ott [15] developed a wave kinetic equation, assuming that the turbulence is weak and the random phase approximation is applicable. From the Maxwell's equations, taking into account the density fluctuations, $\delta n/n$ (here, δn and n are the density fluctuations and the equilibrium density, respectively), one find that the electric field $\mathbf{E}(\mathbf{x},t) = \mathbf{E}(\mathbf{x};\omega)\mathrm{e}^{-i\omega t}$ (harmonic dependence on time) satisfies the wave equation

$$\nabla \times \nabla \times \mathbf{E}(\mathbf{x};\omega) - \left(\frac{\omega}{c}\right)^2 \boldsymbol{\varepsilon} \cdot \mathbf{E}(\mathbf{x};\omega) = \left(\frac{\omega}{c}\right)^2 \frac{\delta n}{n}(\boldsymbol{\varepsilon} - \mathbf{I}) \cdot \mathbf{E}(\mathbf{x};\omega), \tag{1}$$

where c is the speed of light in free space, $\boldsymbol{\varepsilon}$ is the cold plasma dielectric tensor given in the absence of density fluctuations and $\mathbf{I}$ is the identity tensor. Fourier transforming equation (1) one obtains

$$\boldsymbol{\Lambda}(\mathbf{k},\omega) \cdot \mathbf{E}(\mathbf{k},\omega) = -\left(\frac{\omega}{c}\right)^2 \sum_{\mathbf{k}',\omega'} \frac{\delta n(\mathbf{k}-\mathbf{k}',\omega-\omega')}{n}(\boldsymbol{\varepsilon} - \mathbf{I}) \cdot \mathbf{E}(\mathbf{k}',\omega') \tag{2}$$

where

$$\boldsymbol{\Lambda}(\mathbf{k},\omega) \equiv \frac{c^2}{\omega^2}(\mathbf{kk} - \mathbf{I}) + \boldsymbol{\varepsilon} \tag{3}$$

is the dispersion tensor. Without density fluctuations, equation (2) reduces to the well-known wave equation $\boldsymbol{\Lambda} \cdot \mathbf{E}(\mathbf{k},\omega) = 0$, in which the wave mode with frequency $\omega = \omega_k$ is

determined by the dispersion relation $\mathbf{D}(\mathbf{k},\omega) = \det|\mathbf{\Lambda}(\mathbf{k},\omega)| = 0$. After introducing the unit polarization vector, $\mathbf{e}(\mathbf{k})$, where $\mathbf{E}(\mathbf{k}) \equiv E(\mathbf{k})\mathbf{e}(\mathbf{k})$, expanding $\mathbf{\Lambda}(\mathbf{k},\omega)$ in equation (2) for $\omega = \omega_{\mathbf{k}} + i\partial/\partial t$ with $\omega_{\mathbf{k}} \gg |\partial/\partial t|$ and contracting the resulting equation with $\mathbf{e}^*(\mathbf{k})$, one finds

$$i\mathbf{e}^*(\mathbf{k}) \cdot \frac{\partial \mathbf{\Lambda}}{\partial \omega} \cdot \mathbf{e}(\mathbf{k}) \frac{\partial}{\partial t} E(\mathbf{k}) = \\ - \frac{\omega_{\mathbf{k}}^2}{c^2} \sum_{\mathbf{k}'} \frac{\delta n(\mathbf{k}-\mathbf{k}')}{n} \mathbf{e}^*(\mathbf{k}) \cdot (\boldsymbol{\varepsilon} - \mathbf{I}) \cdot \mathbf{e}(\mathbf{k}') E(\mathbf{k}'), \tag{4}$$

where use has been made of the fact that $\mathbf{e}^*(\mathbf{k}) \cdot \mathbf{\Lambda}(\omega_{\mathbf{k}}, \mathbf{k}) = 0$. In equation (4), the frequency shift ω' introduced by the density fluctuations is neglected since the frequency of the lower hybrid wave ($\sim$ GHz) is much larger than the frequency of the density fluctuations of interest (< 1 MHz) in this work. Bonoli and Ott [15], then introduce the wave energy density,

$$u(\mathbf{k}) = \frac{\omega_{\mathbf{k}}}{8\pi} \mathbf{e}^*(\mathbf{k}) \cdot \frac{\partial \mathbf{\Lambda}}{\partial \omega} \cdot \mathbf{e}(\mathbf{k}) |E(\mathbf{k})|^2 \tag{5}$$

so that equation (4) can be rewritten in terms of $C(\mathbf{k}) = |u(\mathbf{k})|^{1/2}$, namely,

$$i\frac{\partial}{\partial t} C(\mathbf{k}) = \sum_{\mathbf{k}'} V(\mathbf{k}, \mathbf{k}', \omega_{\mathbf{k}}) \frac{\delta n(\mathbf{k}-\mathbf{k}')}{n} C(\mathbf{k}') \tag{6}$$

where

$$V(\mathbf{k}, \mathbf{k}', \omega_{\mathbf{k}}) = -\frac{\omega_{\mathbf{k}}}{2} \frac{\mathbf{e}_{\mathbf{k}}^* \cdot (\boldsymbol{\varepsilon} - \mathbf{I}) \cdot \mathbf{e}_{\mathbf{k}'}}{\sqrt{\mathbf{e}_{\mathbf{k}}^* \cdot \mathbf{M} \cdot \mathbf{e}_{\mathbf{k}}} \sqrt{\mathbf{e}_{\mathbf{k}'} \cdot \mathbf{M} \cdot \mathbf{e}_{\mathbf{k}'}}} \tag{7}$$

with the matrix $\mathbf{M}$ being defined by

$$\mathbf{M} = \frac{1}{2} \omega_{\mathbf{k}} \frac{\partial \mathbf{\Lambda}}{\partial \omega}. \tag{8}$$

By the application of the random phase approximation to equation (6) together with an integration over continuous $\mathbf{k}$ instead of a sum of discrete wavenumbers, we arrive at the wave kinetic equation of Bonoli and Ott [15]:

$$\frac{dF}{dt} + 2\gamma F = \\ \sum_{\sigma=\mathrm{S,F}} \int_0^{2\pi} K(k'_{\perp\sigma}, k_\perp, \beta) S(\kappa_\sigma) [F(\phi+\beta) - F(\phi)] \mathrm{d}\beta \tag{9}$$

where

$$K(k'_{\perp\sigma}, k_\perp, \beta) = \frac{2\pi k'_{\perp\sigma}}{V_{g_{\perp}\sigma}} |V(k'_{\perp\sigma}, k_\perp, \beta, \omega_{\mathbf{k}})|^2. \tag{10}$$

For additional details of the derivation of equation (9) the reader is referred to the Appendix of [15] and [18, 19, 20]. However, some explanation of the terms in equation (9) is required here. In order to derive equation (9), it has been assumed that the frequency and the parallel wavenumber of the low-frequency fluctuations are neglected with respect to ω and $k_\parallel$ of the LH wave, respectively. Therefore, ω and $k_\parallel$ are conserved

during the scattering. This assumption is fulfilled for the particular cases of interest; in fact, the density fluctuations along the magnetic field are typically mostly homogeneous. In equation (9), terms β and κ_σ result from a transform coordinate in evaluating the integral in equation (6). In particular, the transformation is from $(k'_{\perp\sigma}, \phi')$ to (κ_σ, β) with

$$\kappa_\sigma = |\mathbf{k}'_{\perp\sigma} - \mathbf{k}_\perp|, \quad \text{and} \quad \beta = \phi' - \phi. \tag{11}$$

Here, β represents the rotation angle of the perpendicular (with respect to the magnetic field) wave vector, $\mathbf{k}_\perp$, during a scattering event, in which

$$\mathbf{k}_\perp \cdot \mathbf{k}'_{\perp\sigma} = k_\perp k'_{\perp\sigma} \cos\beta, \tag{12}$$

where $\mathbf{k}'_{\perp\sigma}$ denotes the perpendicular wave vector after a rotation. In equation (12), $k_\perp \equiv |\mathbf{k}_\perp|$ and $k'_{\perp\sigma} \equiv |\mathbf{k}'_{\perp\sigma}|$ are obtained from the respective dispersion relation according to the mode in which the wave scatters. Like-mode scattering (slow $\rightarrow$ slow or fast $\rightarrow$ fast) and unlike-mode scattering (slow $\rightarrow$ fast or fast $\rightarrow$ slow) are both taken into account in the model. In fact, in equation (9), the summation over σ, with $\sigma = \mathrm{S}, \mathrm{F}$ denoting the slow and fast wave roots of the dispersion relation, includes possible mode conversion between the fast and slow waves. F ($\equiv C_{\mathbf{k}} C^*_{\mathbf{k}}$) and d/dt operator represent the wave energy density and the conservative Lagrangian derivative following the ray, respectively; γ is the electron Landau wave damping. Furthermore, in the integrand of equation (9), $F(\phi + \beta)$ corresponds to the increase of the wave energy density $F(\phi)$ due to the scattering at $\phi + \beta$, while $F(\phi)$ corresponds to the attenuation of the wave energy density $F(\phi)$ due to the scattering. $V_{g_\perp\sigma}$, in equation (10), is the perpendicular component (with respect to the magnetic field) of the group velocity. Finally, in equation (9), $S(\zeta)$ is the perpendicular (with respect to the magnetic field) density fluctuation wave-number spectrum, which is related to the mean-square density fluctuations by [15, 18, 19]

$$\left\langle \left(\frac{\delta n}{n}\right)^2 \right\rangle \equiv 2\pi \int_0^\infty \mathrm{d}\zeta \zeta S(\zeta). \tag{13}$$

$S(\zeta)$ is assumed to be isotropic in the plane perpendicular to the magnetic field and is here approximated by a Gaussian [15, 21]

$$S(\zeta) = \frac{1}{\pi\zeta_0^2} \left\langle \left(\frac{\delta n}{n}\right)^2 \right\rangle \exp\left(\frac{-\zeta^2}{\zeta_0^2}\right) \tag{14}$$

where ζ_0 is related to the fluctuation correlation length λ_c of the density fluctuations, such as $\zeta_0 = 2\pi/\lambda_\mathrm{c}$.

2.2. Validity of the wave kinetic equation

The scattering model described above is characterized by the wave kinetic equation (9), which has been obtained by applying a random phase approximation. From previous

analysis [15, 18, 19], the validity of equation (9) is predicated on the following conditions:

$$\text{if} \quad (k_\perp/\zeta_0)^2 \gg 1 \quad \text{then} \quad \zeta_0 l_s (k_\perp/\zeta_0)^{-2} > 1 \tag{15}$$

$$\text{if} \quad k_\perp \lesssim \zeta_0 \quad \text{then} \quad \zeta_0 l_s > 1 \tag{16}$$

where l_s is the scattering length that corresponds to the distance that the wave must propagate in order that $\mathbf{k}_\perp$ rotates by an angle of 90°. More specifically, the scattering length is defined by $l_s = V_{g\perp}/\nu_1$ where ν_1 is given by [15]

$$\nu_p = 2\int_0^{2\pi} \mathrm{d}\beta K(k_\perp, \beta) S(\kappa) \sin^2\left(\frac{p\beta}{2}\right) \tag{17}$$

with $p = 1$. It is a measure of the damping due to scattering of the lower order ($p = 1$) harmonic of the wave energy density F. Conditions (15) and (16) are evaluated as the ray is scattered in the subroutine implemented in `GENRAY` as a check of the validity of the numerical results.

2.3. Monte Carlo solution to the wave kinetic equation

The wave kinetic equation (9) is solved here by using a Monte Carlo technique, following the work of Bonoli and Ott [15]. Assume that $P(\beta)\mathrm{d}\beta\mathrm{d}t$ represents the probability that a scattering event occurs in an angle between β and $\beta + \mathrm{d}\beta$ in a time interval $\mathrm{d}t$, where

$$P(\beta) = \sum_{\sigma=\mathrm{S,F}} K(k_{\perp\sigma}, \beta) S(\zeta) \equiv \sum_{\sigma=\mathrm{S,F}} P_\sigma(\beta) \tag{18}$$

according to equation (9). The Monte Carlo integration of the wave kinetic equation is accomplished as follows:

(i) choose a time interval Δt so that the total probability of scattering with any angle is small, namely,

$$p = \Delta t \sum_{\sigma=\mathrm{S,F}} \int_0^{2\pi} \mathrm{d}\beta P_\sigma(\beta) \equiv p_S + p_F \ll 1. \tag{19}$$

Condition (19) is assumed in order to avoid multiple scattering events during the time interval Δt.

(ii) make use of the ray tracing code `GENRAY`, generalized to include the scattering model described above, to advance the position of the ray by integrating equation (9) over the time interval Δt.

(iii) adopt a Monte Carlo procedure to describe the effects of the density fluctuations. For illustrative purposes, assume that the wave is propagating in the slow mode before the scattering event and generate a random number X_{random} from a uniform probability distribution on the interval $[0, 1]$. Then, three possibilities can occur:

a) if $0 \le X_{\mathrm{random}} < p_{\mathrm{S}}$ then the wave is scattered into another slow wave (like-mode scattering: slow $\rightarrow$ slow)

b) if $p_{\mathrm{S}} \le X_{\mathrm{random}} < p_{\mathrm{S}} + p_{\mathrm{F}}$ then the wave is scattered into a fast wave (unlike-mode scattering: slow $\rightarrow$ fast)

c) if $X_{\rm random} > p_{\rm S} + p_{\rm F}$ then the wave is not scattered.

(iv) If no scattering occurs in step (iii) then one goes back to step (ii).

(v) If scattering occurs in step (iii) according to conditions (a) and (b) then a random scattering angle β is generated from the distribution

$$G_\sigma(\beta) = \frac{P_\sigma(\beta)}{\int_0^{2\pi} \mathrm{d}\beta P_\sigma(\beta)}. \tag{20}$$

and a new value of $\mathbf{k}'$ after the scattering event is calculated by using the following equations

$$\begin{aligned} k'_\phi &= k_\parallel b_\phi + \frac{k'_\perp}{k_\perp}[(k_\phi - k_\parallel b_\phi)\cos\beta + (k_z b_r - k_r b_z)\sin\beta], \\ k'_z &= \frac{b_r(k_\perp k'_\perp \cos\beta + k_\parallel^2) - k_r k_\parallel - k'_\phi(k_\phi b_r - k_r b_\phi)}{k_z b_r - k_r b_z}, \\ k'_r &= \frac{k_\parallel - k'_z b_z - k'_\phi b_\phi}{b_r}. \end{aligned} \tag{21}$$

These equations provide the new components of $\mathbf{k}'$ after a scattering event, as a function of the component of the wave vector, $\mathbf{k}$, before scattering, assuming that during the scattering $k_\parallel$ is conserved and a rotation of $k_\perp$ by an angle β occurs according to equation (12). In equations (21), $\mathbf{b} \equiv \mathbf{B}/|\mathbf{B}|$ is the unit vector in the direction of the magnetic field and the value of $k'_\perp$ is obtained from the appropriate (slow or fast mode according to the kind of scattering event) dispersion relation.

(vii) The entire process is repeated (steps (ii)-(v)), until all of the power in the ray has been damped.

The procedure described above is performed in order to obtain the energy deposition profile for one particular realization of the random scattering process. The average energy deposition profile is then obtained by performing N different realizations of the random scattering process, using N different random number seed for each scattering event. In principle, in the limit $N \to \infty$ and $\Delta t \to 0$, a Monte Carlo type solution of the wave kinetic equation (9) is performed. It is crucial to recognize that, although $k_\parallel$ is conserved during the scattering event itself as mentioned above (see steps (iii)-(v)), $k_\parallel$ can be modified through the poloidal field because the rotation of $k_\perp$ induces a finite poloidal mode number.

3. Numerical results

The scattering model presented above has been implemented in the ray tracing code `GENRAY` [10], which has been generalized recently to include a 2D model for the scrape-off layer (SOL). More specifically, an exponential decay of the density from its value on the LCFS is included with a density decay length, $\sigma_{\rm n}$ (as input) which is a function of poloidal angle. In addition, an exponential decay of the temperature from its value on the LCFS is also implemented with a temperature decay length, $\sigma_{\rm T}$ (as input). The

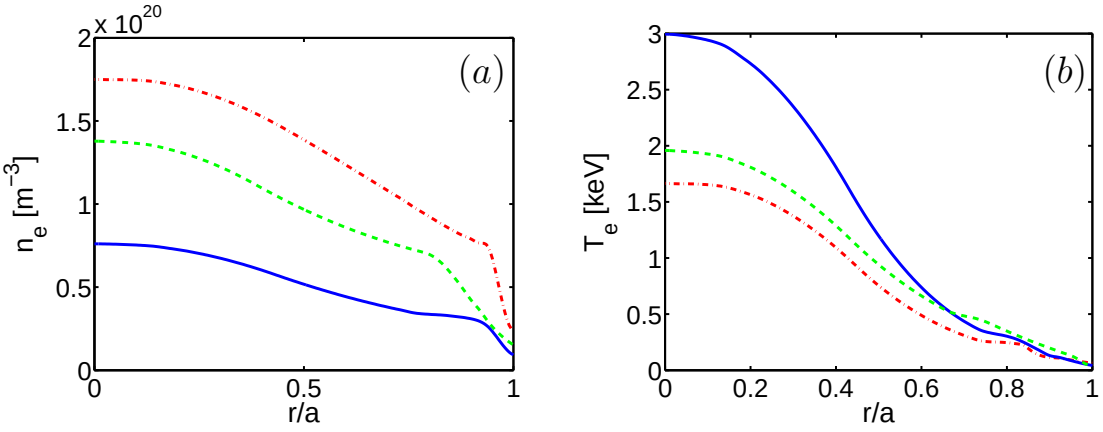

Figure 1. Electron density (a) and electron temperature (b) profiles of Alcator C-Mod discharges with line averaged density equal to $\bar{n}_e = 0.53 \times 10^{20}$ m^{-3} (solid blue curve), $\bar{n}_e = 0.97 \times 10^{20}$ m^{-3} (dashed green curve) and $\bar{n}_e = 1.47 \times 10^{20}$ m^{-3} (dashed-dotted red curve).

2D SOL model, used in this numerical analysis, includes the C-Mod vacuum vessel and the reflection of the ray trajectory from the metallic surface. Furthermore, collisional damping are implemented in `GENRAY` both inside the separatrix and in the SOL region, by replacing the electron mass m_e with $m_e(1 + i\nu_{ei}/\omega)$ in the cold plasma dispersion relation, where ν_{ei} is the effective electron-ion momentum collision frequency [2, 3]. The magnetic field structure from the magnetic axis to the vessel boundary is imported from a magnetic field equilibrium reconstruction [22]. The measured density and temperature profiles on the closed flux surfaces within the separatrix are provided. For more details on the 2D SOL model implemented in `GENRAY`, the reader is referred to [3, 23].

Plasma parameters and equilibria, adopted in these numerical calculations, model a series of Alcator C-Mod discharges in which the discrepancies between the measured and predicted hard x-ray emission increase at the higher densities [3]. In Figure 1, the electron density and temperature as a function of the normalized minor radius r/a are shown for three cases, corresponding to a line averaged density $\bar{n}_e = 0.53 \times 10^{20}$ m^{-3} (low density, shown in solid blue curve in Figure 1), $\bar{n}_e = 0.97 \times 10^{20}$ (mid density, shown in dashed green curve in Figure 1), and $\bar{n}_e = 1.47 \times 10^{20}$ m^{-3} (high density, shown in dashed-dotted red curve in Figure 1). With regard to the SOL parameters, the density decay length, σ_n varies between 0.1 m in the divertor regions and 0.02 m on the outer midplane. The temperature decays length σ_T is of 0.005 m until the temperature reaches a minimum value of 5 eV, beyond which the plasma temperature remains constant. These values are typical for Alcator C-Mod L-mode discharges [3]. In addition, the effective charge of the plasma in the SOL is assumed to be $Z_{eff} = 1.8$. This parameter has been chosen, within the experimental data range, to emphasize more scattering than collisional damping effects (being $\nu_{ei} \propto n_e Z_{eff} T_e^{-1.5}$) [3, 28].

The radial density fluctuations profile necessary for solving equation (9) has been

chosen such that

$$\frac{\delta n(r)}{n} = \begin{cases} \left(\frac{r}{a}\right) f_1 + f_2, & 0.8 \leq \frac{r}{a} < \text{launching point}; \\ 0, & \text{for } 0 \leq \frac{r}{a} < 0.8. \end{cases} \tag{22}$$

where f_1 and f_2 are chosen so that $\delta n/n = 40\%$ at launching point and $\delta n/n = 2.5\%$ at $r/a = 0.8$; the fluctuations correlation length, λ_c, is taken to be 0.5 cm and 1 cm. These parameters are based on the Alcator C-Mod experimental observations [24, 25, 21, 26].

3.1. Scattering effects on ray trajectories and $N_\parallel$ evolution

Figures 2 and 3 illustrate the main possible effects of scattering on a single ray trajectory in the low (see solid blue curve in Figure 1) and high density (see dashed-dotted red curve in Figure 1) parameter regimes, respectively. The initial value of the parallel refractive index is $N_\parallel = -1.5$ and the fluctuation correlation length is $\lambda_c = 1$ cm. Both Figure 2 (low density) and 3 (high density) show three possible paths for the scattered rays, obtained by using three different seeds in the Monte Carlo simulations. Note that ray trajectory terminates when the power is fully absorbed.

In these density regimes, scattering may either to enhance penetration of the ray in the good confinement region (cf. Figures 2(a) for low density and 3(a) for high density) or to keep the ray longer on the edge of the plasma (Figures 2(c) and 3(c)) or even in the SOL (cf. Figure 3(b)). In addition, one can note that for low density case (Figures 2(a)-(c)) the ray trajectories are basically inside of the LCFS (apart from the beginning of the rays propagation); on the other hand, for high density case (Figures 3(a)-(c)) the ray trajectories initially linger at or outside the LCFS. A more systematic analysis with good statistics for the scattering calculations by using a large number of rays will be utilized in the remaining of this paper. With regard to the evolution of $N_\parallel$ along the ray, Figures 4 and 5 show $N_\parallel$ as a function of the poloidal distance along the ray for the trajectories shown in Figure 2 and 3, respectively. It appears that scattering generally induces a quite significant $N_\parallel$ upshift when the scattering enhances the ray penetration into the plasma core. When the ray either stays longer in the edge plasma region or has a long path before power is fully absorbed, the profile of $N_\parallel$ has several oscillations around its initial value. This is in part because the ray receives random kicks that increase and decrease the $N_\parallel$ value during the scattering events.

3.2. Scattering effects on the power density profile

Another important aspect to be investigated is the impact of the scattering on the power absorption profile. Here, ray tracing together with Fokker-Planck calculations, obtained with the generalization of `GERNAY/CQL3D` package, show how scattering can affect the power absorption profile when taking into account the 2D SOL region. While the 2D SOL region is included in the ray tracing calculations, it is important to note that this region is not directly included in `CQL3D`. Therefore, the quasilinear diffusion coefficient is not evaluated outside of the LCFS for the Fokker-Planck calculations. Hence, the

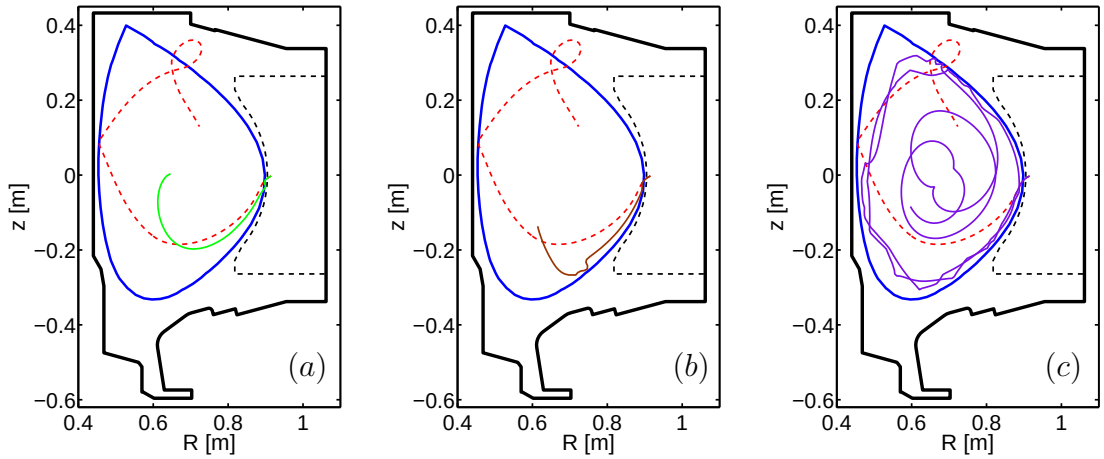

Figure 2. Poloidal ray trajectories for an Alcator C-Mod discharge at low density ($\bar{n}_e = 0.53 \times 10^{20}$) including a 2D SOL model. Dashed (red) curve represents the ray trajectory without scattering while the solid curves represents three different realizations of scattering, shown in (a), (b), and (c), for $\lambda_c = 1$ cm. The initial value of $N_{\|}$ is -1.5. Alcator C-Mod vacuum vessel (solid black line) and the separatrix (solid blue line) are also shown for reference. Limiter geometry (dashed black line) is shown although is not included in the simulation.

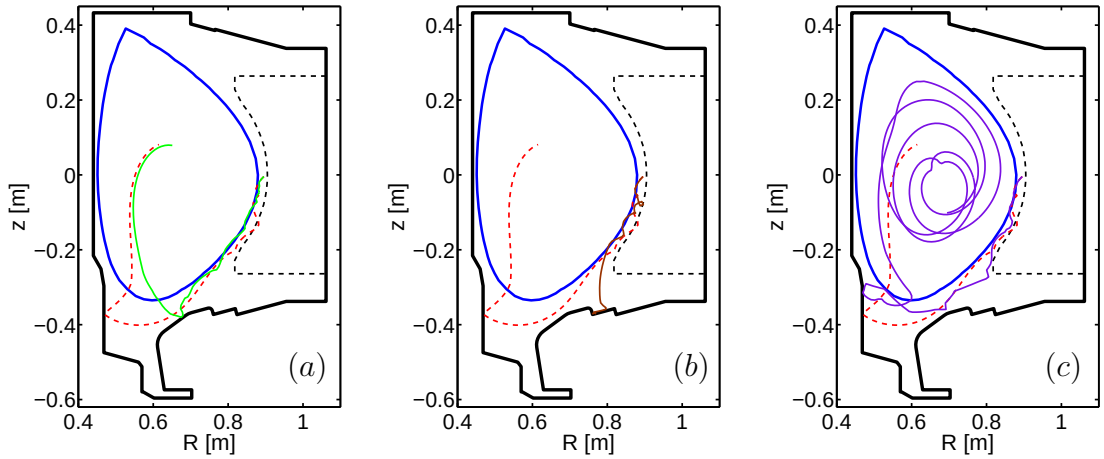

Figure 3. Poloidal ray trajectories for Alcator C-Mod discharge at high density ($\bar{n}_e = 1.47 \times 10^{20}$) including a 2D SOL model. Dashed (red) curve represents the ray trajectory without scattering while the solid curves represents three different realizations of scattering, shown in (a), (b), and (c), for $\lambda_c = 1$ cm. The initial value of $N_{\|}$ is -1.5. Alcator C-Mod vacuum vessel (solid black line) and the separatrix (solid blue line) are also shown for reference. Limiter geometry (dashed black line) is shown although is not included in the simulation.

power available for damping within the SOL depends on the amount of power lost in the SOL, due to collision. This reduced power is used in the `CQL3D` calculations within

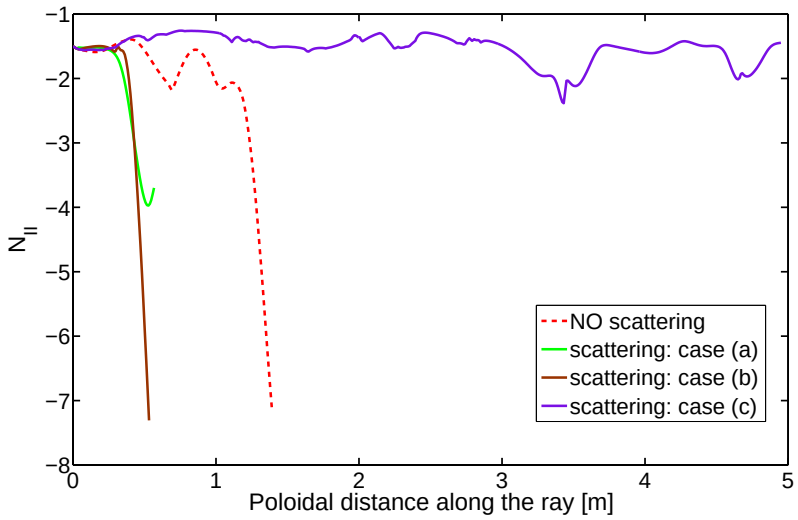

Figure 4. Parallel (with respect to the magnetic field) refractive index, $N_{\|}$, as a function of the poloidal distance along the ray. Dashed (red) curve represents the $N_{\|}$ evolution without scattering while the solid curves represents the $N_{\|}$ evolution of three different realizations of scattering corresponding to the three ray trajectories shown in Figure 2(a), 2(b), and 2(c), respectively, for low density case. The initial value of $N_{\|}$ is -1.5.

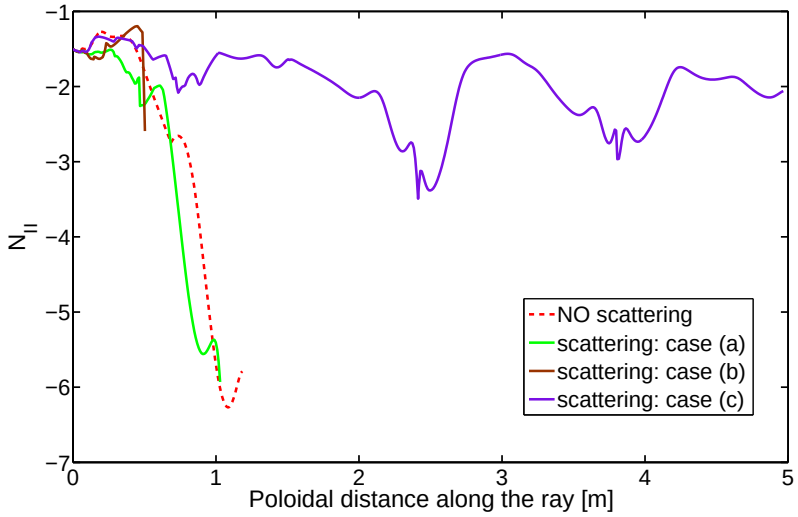

Figure 5. Parallel (with respect to the magnetic field) refractive index, $N_{\|}$, as a function of the poloidal distance along the ray. Dashed (red) curve represents the $N_{\|}$ evolution without scattering while the solid curves represents the $N_{\|}$ evolution of three different realizations of scattering corresponding to the three ray trajectories shown in Figure 3(a), 3(b), and 3(c), respectively, for high density case. The initial value of $N_{\|}$ is -1.5.

the separatrix region.

In order to simulate LHCD on Alcator C-Mod and to have good statistics for the

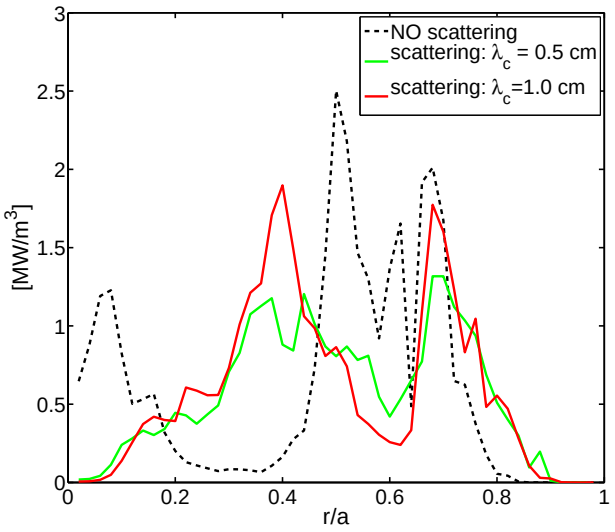

Figure 6. Power absorption profile as a function of the normalized minor radius, r/a, calculated by `GENRAY/CQL3D` for an Alcator C-Mod discharge at $\bar{n}_e = 0.53 \times 10^{20}$ m^{-3}. Power damping profile without scattering is shown in dash (black) curve while two different scattering cases are shown in green and red curves, corresponding to a fluctuation correlation length $\lambda_c = 0.5$ cm and 1 cm, respectively.

scattering calculations, the LH antenna is modeled with two "grills", one launching waves in the current drive direction with $N_\parallel = -1.5$ to -2.4, peaked at $N_\parallel = -1.9$ and one in the counter current drive direction with $N_\parallel = 6.9$ to 7.8, peacked at $N_\parallel = 7.4$. Each grill has four rows (to model the real LH antenna) distributed across the height of the antenna. For each row there are 15 rays in the current drive direction and 4 in the counter current drive direction. In addition, all rays are launched from outside the LCFS, in particular, for $r/a = 1.05$. To evaluate the scattering effects, twenty different simulations are produced, each with a unique random seed in the scattering model. For each seed, a `GENRAY` run including scattering effects is performed obtaining all ingredients needed for the evaluation of the quasilinear diffusion coefficient in the Fokker-Planck calculations. Then, for each specific seed (i.e., for each specific `GENRAY`'s output) an iteration with `CQL3D` in order to reach a steady state is performed in order to evaluate the electron distribution function and the power density profile. Finally, an average of the power density profiles, obtained with this procedure, is performed and compared with the power density profile evaluated without scattering. It is important to mention that twenty different scattering realizations (namely, twenty different random seeds) together with the large number of rays considered for modeling the LH wave beam, mentioned above, result to be a good ensemble in solving the wave kinetic equation 9. In fact, no significant changes in the power density profile are found increasing the number of random seeds.

The results of the numerical procedure described above indicate that a general broadening of the power deposition results from the wave scattering. Figures 6 and

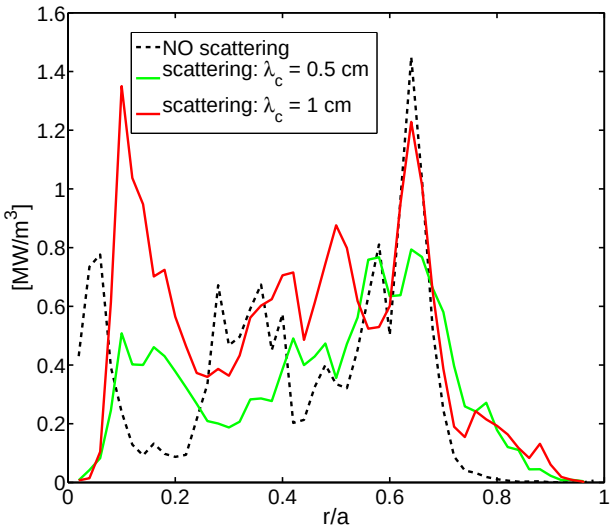

Figure 7. Power absorption profile as a function of the normalized minor radius, r/a, calculated by `GENRAY/CQL3D` for an Alcator C-Mod discharge at $\bar{n}_e = 1.47 \times 10^{20}$ m^{-3}. Power damping profile without scattering is shown in black curve while two different scattering cases are shown in green and red curves, corresponding to a fluctuation correlation length $\lambda_c = 0.5$ cm and 1 cm, respectively.

7 show the power absorption profiles as a function of the normalized minor radius, r/a, with and without scattering for Alcator C-Mod discharges at low density ($\bar{n}_e = 0.53 \times 10^{20}$ m^{-3}) and high density ($\bar{n}_e = 1.47 \times 10^{20}$ m^{-3}), respectively. The dashed (black) curve represents the power density profile without scattering while the solid curves include the effects of scattering. Two different fluctuation correlation lengths are plotted: $\lambda_c = 0.5$ cm (green curve) and 1 cm (red curve) both for low and high density cases. For the low density case (cf. Figure 6), scattering seems to have basically two effects on the power density profile: (i) a broadening and redistribution of the power density as a function of r/a and (ii) a reduction of the power density near the magnetic axis of the plasma. In addition, it appears that the integrated power within $r/a < 1$ is less for the case with the shorter fluctuation correlation length (see green curve with respect to red curve). For the high density regime (cf. Figure 7), a radial redistribution of the power density is once again found, though a less of reduction of the power density near the magnetic axis is less pronounced than in the low density case. The integrated power absorbed with $\lambda_c = 0.5$ cm is smaller than with $\lambda_c = 1$ cm case, as in the low density regime. Furthermore, for $\lambda_c = 1$ cm, it appears that the integrated power within the separatrix is larger than in the case without scattering. This may be due in part to a $k_\parallel$ upshift together with a better core penetration (as shown in the previous subsection) induced by the scattering in the SOL region.

3.3. Comparison between Hard X-ray data from Alcator C-Mod and `GENRAY/CQL3D` *simulations*

In recent experiments on LHCD in Alcator C-Mod [3, 27, 28], a strong interaction between LH waves and SOL region has been found together with a significant drop in the LHCD efficiency at high electron density plasmas. These observations are now referred to as the "density limit" effect. Furthermore, in these studies it has been shown that collisional damping effects in the SOL region can contribute to decrease the LHCD efficiency at high density plasma, although collisional damping alone does not seem to be sufficient to fully reproduce so strong a drop in the LHCD efficiency for the highest density cases. Collisional damping effects are included in the ray tracing/Fokker-Planck numerical code both inside the separatrix, where collisional damping is typically smaller than Landau damping, and in the SOL region, where collisional damping is more significant due to the low temperature in this region.

Here, simulations of the effects of wave scattering in LHCD experiment in Alcator C-Mod, with and without collisional damping, are used to evaluate if wave scattering effects can contribute significantly to the loss in the LHCD efficiency at high density. A direct measure of the validity of the simulations is the degree of agreement between the measured and simulated x-ray spectrum emission generated during the LH pulse in the plasma discharge. `CQL3D` includes a fast electron bremsstrahlung x-ray synthetic diagnostic, the output of which can be directly compared with the hard x-ray (HXR) emission measured in the experiment.

Figure 8 shows a comparison between the Alcator C-Mod experimental observations and the numerical results obtained from `GENRAY/CQL3D` simulations. The green circles correspond to the experimental HXR count rates for L-mode discharges at 800 kA and 5.4 T with a bremsstrahlung emission in the 40-200 keV range [3, 27, 28]. Chords 9-24 of a 32-chord poloidally viewing HXR diagnostic on Alcator C-Mod [29] have been used to determine the non-thermal electron population in the plasma core [3]. In Figure 8, three numerical simulations are shown: a case without collisional damping and scattering effects, shown in dashed black line, and two cases including only scattering effects with two different fluctuation correlation lengths: $\lambda_c = 0.5$ cm (shown in dashed green line) and 1 cm (shown in red line). From Figure 8, one can clearly see that the numerical results without collisional damping and scattering follow the expected $\sim 1/n_e$ behavior, as predicted from the theory [30, 31] and already shown in Wallace *et al* [3]. At the same time, it appears that including only scattering effects does not to capture the behavior of the experimental HXR emission. Only a small deviation from the case without collisional damping and scattering is noted. Moreover, no significant differences in the predictions are seen using the two fluctuation correlation lengths. Error bars, for the scattering cases, indicate a standard deviation from the average value obtained by following the numerical procedure described in the subsection 3.2, using twenty different scattering realizations. In these numerical simulations, a mid density case ($\bar{n}_e = 0.97 \times 10^{20}$ m^{-3}) has been considered together with the low ($\bar{n}_e = 0.53 \times 10^{20}$ m^{-3}) and high density

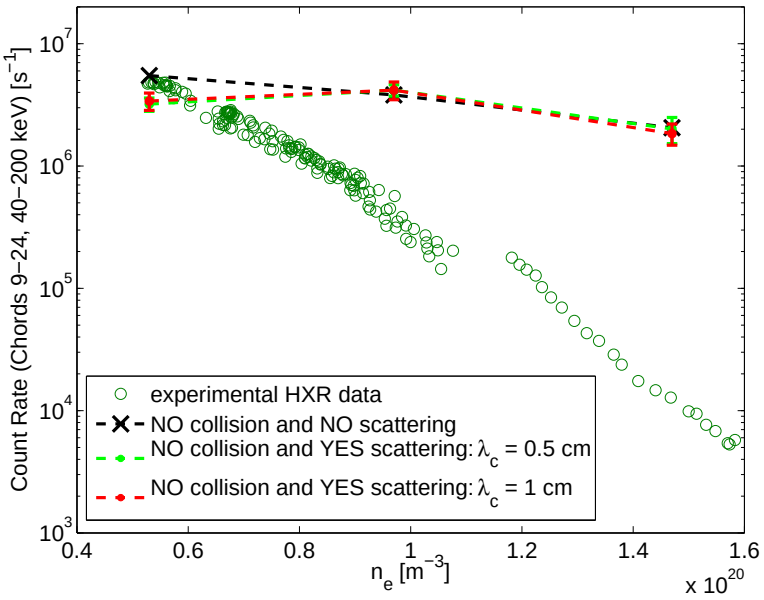

Figure 8. Comparison between the hard x-ray (HXR) emission from Alcator C-Mod experiment and the simulated (HXR) emission from `GENRAY/CQL3D` as a function of the line averaged density. Green circles indicate the experimental HXR count rates for L-mode discharges at 800 kA and 5.4 T [3, 27, 28]. The dashed lines represent HXR emission predicted by `GENRAY/CQL3D`. Results shown in dashed black line represent the case without both collisional damping and scattering effects. The dashed green and red lines take into account only scattering effects with $\lambda_c = 0.5$ cm and 1 cm, respectively. Error bars in the green and red lines indicate a standard deviation from the average value obtained by making use of twenty different scattering realizations.

($\bar{n}_e = 1.47 \times 10^{20}$ m^{-3}) cases already presented in subsection 3.1 and 3.2. For the low density case, scattering effects seem to slightly reduce the HXR count rates; on the other hand, for the mid and high density cases, scattering effects introduce only a small perturbation with respect to the case without scattering and collisional damping (note that Figure 8 has a logarithmic scale). Predictions of the hard x-ray spectrum obtained by combining collisional damping and scattering effects are compared in Figure 9 to the experimental observations. The simulated spectrum obtained by taking into account only collisional effects is shown in dashed black line, as well as predictions from two additional cases that include both collision and scattering for $\lambda_c = 0.5$ cm (green line) and 1 cm (red line). From this figure, it appears that scattering added to collisional damping only slightly reduces the drop in LHCD efficiency for the high density case with the shorter fluctuation correlation length ($\lambda_c = 0.5$ cm). Therefore, though scattering can enhance collisional damping in the edge of the plasma, it does not appear to be strong enough to reproduce the experimental results. Low and mid density cases, with collision and scattering included, have a behavior similar to the results shown in Figure 8 although, of course, with a smaller HXR count rates mainly due to collisional damping effects. For high density case, unlike Figure 8, error bars are larger for both fluctuation

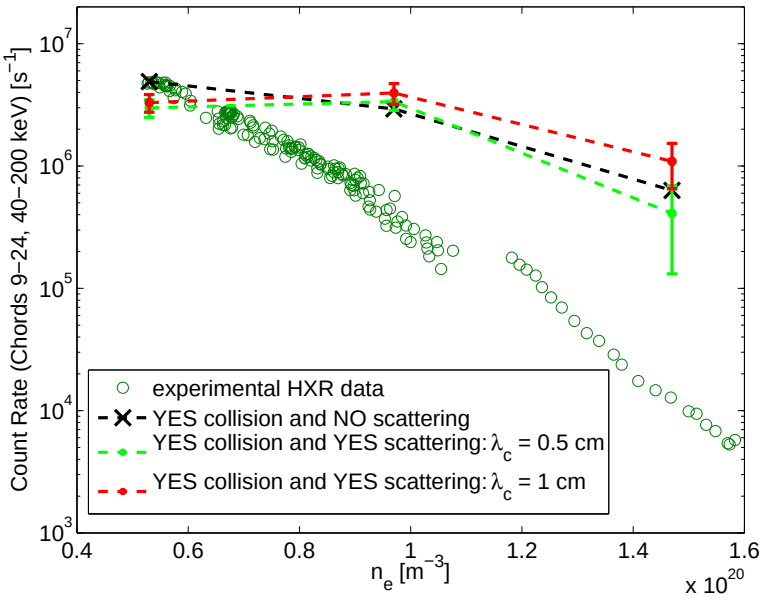

Figure 9. Comparison between the hard x-ray (HXR) emission from Alcator C-Mod experiment and the simulated (HXR) emission from `GENRAY/CQL3D` as a function of the line averaged density. Green circles indicate experimental HXR count rates for L-mode discharges at 800 kA and 5.4 T [3, 27, 28]. The dashed lines represent HXR emission predicted by `GENRAY/CQL3D`. Results shown in dashed black line represent the case with only collisional damping effects considered. The dashed green and red lines take into account both collisional damping and scattering effects with $\lambda_c = 0.5$ cm and 1 cm, respectively. Error bars in the green and red lines indicate a standard deviation from the average value obtained by making use of twenty different scattering realizations.

correlation lengths, probably due to a stronger interplay between collision and scattering in the SOL region with the low temperature and relatively high density. Moreover, the shorter correlation length case ($\lambda_c = 0.5$ cm) shows a larger reduction in HXR count rates with respect to the $\lambda_c = 1$ cm case, in agreement with the power density profiles analyzed in subsection 3.2. A reason why scattering effects in combination with collisional damping do not seem to explain the drop in the LHCD efficiency, might be the fact that Alcator C-Mod discharges are commonly in the multi-pass regime (in particular, the discharges presented and analyzed in this work). Therefore, the already stochastic behavior of the rays is less sensitive to the scattering induced by the edge density fluctuations. In other words, scattering effects act as a additional perturbation to the rays trajectories but they are not able to induce any really significant differences to the already chaotic behavior of the ray paths obtained in the multi-pass regime, at least in this specific numerical analysis. In fact, it is important to note that the ray tracing formalism may have limits of applicability, in particular, in the frequency range corresponding to LH waves and in the multi-pass regime [32, 33]. Numerical results shown here, together with their interpretation, are in agreement with the work of

Peysson *et al* [12], where the electron density fluctuations are described with a statistical model.

4. Summary and discussion

In this work, the effects of scattering induced by the edge density fluctuations on the LH wave propagation and absorption have been evaluated by comparing a ray tracing/Fokker-Plack simulations against Alcator C-Mod experiments. The scattering model adopted in this numerical analysis, which utilizes a wave kinetic equation developed by Bonoli and Ott [15], has been described. This equation has been implemented in the ray tracing code `GENRAY` and solved by a Monte Carlo technique. Evaluation of the scattering effects on the LH wave propagation with the ray tracing/Fokker Planck code package `GENRAY/CQL3D` including a SOL region and a scattering model for Alcator C-Mod discharges, in a multi-pass regime, has been performed. This numerical analysis illustrates and quantifies the consequences of scattering effects on LH wave propagation and absorption for low and high density discharges. It has been found that scattering effects can either enhance the core penetration of LH waves, due to a $k_{\|}$ upshift, or inhibit the wave penetration, keeping the LH rays on the edge of the plasma. With regard to the impact of scattering on the power absorption profile, the main conclusion is that scattering generally induces a broadening and a redistribution of the power density profile. In addition, scattering induced by fluctuations with shorter correlation length tends to further reduce the power available for current drive and profile control in the plasma within the LCFS. On the other hands, a $k_{\|}$ upshift induced by the scattering results in an increase of the power available within the LCFS.

A detailed comparison between the fast bremsstrahlung electron emission measured in Alcator C-Mod experiment for L-mode discharges at 800 kA and 5 T [3, 27, 28] and the numerical results including scattering, obtained from the hard x-ray synthetic diagnostic implemented in `CQL3D`, has been also presented and discussed. Based on the simulations presented here, scattering effects alone are not able to reproduce the observed steep decrease in LHCD efficiency at high density plasmas in the experiment on Alcator C-Mod. Only a small deviation in the HXR count rates from the case without scattering has been found. On the other hand, by combining collisional damping with scattering effects, a reduction of the HXR emission for high density plasma is found, for scattering by density fluctuations characterized with a shorter correlation length. Therefore, scattering seems to enhance the collisional damping, reducing the LHCD efficiency. Although such scattering effects, combined with collisional damping, seem to go in the direction to improve the agreement with the experimental data, they do not appear to be the dominant physical mechanism that causes the decrease in LHCD efficiency observed in experiments on Alcator C-Mod in the multi-pass regime. However, in [28] has been shown that the collisional damping effects alone with an higher Z_{eff} value tend to further reduce the disagreement with the experimental data. A reason why the

impact of the scattering effects on the LH wave propagation and absorption may not play the major role in causing the observed "density limit" is that, in the multi-pass regime, the stochastic behavior of the rays is so pronounced that additional stochasticity induced by wave scattering is not significant. In other words, wave scattering due to density fluctuations certainly contributes to either enhancing the collisional damping or helping the core penetration at the edge of the plasma but, within this model, it cannot play a really major role. Such result is, indeed, in agreement with the recent work of Peysson *et al* [12] where a fluctuating layer model, based on electron drift wave turbulence, has been developed. Finally, it is important to mention that this conclusion is intrinsically related to the fact that LH wave propagation and absorption are commonly evaluated within the ray tracing (or geometrical optics) formalism. The use of the ray tracing method for waves in the LH frequency range, in particular, in the multi-pass regime, is, indeed, in the limit of its applicability [32, 33]. Some recent attempts to describe a scattering model by the edge electron density fluctuations in the full-wave formalism have been presented [34], but the primary cause of the observed "density limit" is still under investigation.

Acknowledgments

This research is supported by the U.S. Department of Energy under contract number DE-AC02-09CH11466.

References

[1] C. Gormezano and et al. *Nucl. Fusion*, 47:S285, 2007.
[2] P. T. Bonoli and R. C. Englade. *Phys. Fluids*, 29:2937, 1986.
[3] G. M. Wallace and et al. *Phys. Plasmas*, 17:082508, 2010.
[4] R. Cesario. *Phys. Rev. Lett.*, 92:175002, 2004.
[5] R. Cesario and et al. *Plasma Phys. Control. Fusion*, 53:085011, 2011.
[6] E. Barbato. *Nucl. Fusion*, 51:103032, 2011.
[7] O. Meneghini. In *Bull. Am. Phys. Soc.*, 2011.
[8] O. Meneghini. PhD thesis, MIT, 2011.
[9] V. Pericoli Ridolfini and et al. *Nucl. Fusion*, 51:113023, 2011.
[10] A. P. Smirnov and R. W. Harvey. In *Bull. Am. Phys. Soc.*, volume 40, page 1837, 1995.
[11] P. L. Andrews and F. W. Perkins. *Phys. Fluids*, 26:2537, 1983.
[12] Y Peysson and et al. *Plasma Phys. Control. Fusion*, 53:124028, 2011.
[13] K. Hizanidis, A.K. Ram, Y. Kominis, and C. Tsironis. *Phys. Plasmas*, 17:022505, 2010.
[14] P. T. Bonoli and E. Ott. *Phys. Rev. Lett.*, 46:424, 1981.
[15] P. T. Bonoli and E. Ott. *Phys. Fluids*, 25:359, 1982.
[16] G Vahala, L. Vahala, and P. T. Bonoli. *Phys. Fluids B*, 4:4033, 1992.
[17] W. Harvey and M. McCoy. In *Proceedings of the IAEA Technical Committee Meeting on Simulation and Modeling of Thermonuclear Plasmas*, page 489, 1992.
[18] E. Ott. *Phys. Fluids*, 22:1732, 1979.
[19] E. Ott, B. Hui, and K. R. Chu. *Phys. Fluids*, 23:1031, 1980.
[20] R. Z. Sagdeev and A. A. Galeev. *Nonlinear Plasma Theory.* Benjamin, New York, 1969.
[21] S. J. Zweben and et al. *Plasma Phys. Control. Fusion*, 49:S1, 2007.
[22] L. L. Lao and et al. *Nucl. Fusion*, 25:1611, 1985.
[23] G. M. Wallace. PhD thesis, MIT, 2010.
[24] B. LaBombard and et al. *Phys. Plasmas*, 8:2107, 2001.
[25] J. L. Terry and et al. *Fusion Sci. and Technol.*, 51:342, 2007.
[26] S. J. Zweben and et al. *Plasma Phys. Control. Fusion*, 54:025008, 2012.
[27] G. M. Wallace and et al. *Nucl. Fusion*, 51:083032, 2011.
[28] G. M. Wallace and et al. *Phys. Plasmas*, 19:062505, 2012.
[29] J. Liptac and et al. *Rev. Sci. Instrum.*, 77:103504, 2006.
[30] N. J. Fisch and A. H. Boozer. *Phys. Rev. Lett.*, 45:720, 1980.
[31] N. J. Fisch. *Rev. Mod. Phys.*, 59:175, 1987.
[32] A. Cardinali and et al. *Phys. Plasmas*, 14:112506, 2007.
[33] A. S. Richardson, P. T. Bonoli, and J. C. Wright. *Phys. Plasmas*, 17:052107, 2010.
[34] K. Hizanidis and et al. In *39th EPS Conf. on Plasma Phys.*, page P2.152, 2012.

The Princeton Plasma Physics Laboratory is operated
by Princeton University under contract
with the U.S. Department of Energy.

Information Services
Princeton Plasma Physics Laboratory
P.O. Box 451
Princeton, NJ 08543

Phone: 609-243-2245
Fax: 609-243-2751
e-mail: pppl_info@pppl.gov
Internet Address: http://www.pppl.gov